Temporal and spatial correlations in a viscoelastic model of heterogeneous faults

Bora Örçal[1] and Ayşe Erzan[1,2]

[1] *Department of Physics, Faculty of Sciences and Letters*
Istanbul Technical University, Maslak 80626, Istanbul, Turkey
[2] *Gürsey Institute, P. O. Box 6, Çengelköy 81220, Istanbul, Turkey*

(February 1, 2008)

We study the temporal and spatial correlations in a one-dimensional model of a heterogeneous fault zone, in the presence of viscoelastic effects. As a function of dynamical weakening and of dissipation, the system exhibits three different "phases" : one in which there are no time correlations between the events, a second, in which there are "Omori's law" type temporal correlations, and a third, runaway phase with quasiperiodic system size events.
PACS numbers 91.30.P, 62.20.F, 62.20.D

I. INTRODUCTION

The spatial and temporal distribution of earthquake activity has been the foremost aim and most successful aspect of earthquake modelling via discerete, nonlinear networks of elastic elements interacting via nearest neighbor couplings, typically loaded at a constant rate far from the fault boundary. The Burridge-Knopoff [1] model has been the forerunner of a series of coarse-grained dynamical models [2–4], which have firmly established the understanding of seismic activity within the paradigm of self-organized criticality [5–7]. These systems exhibit "subcritical" or "supercritical" deviations [3] from strict self-similarity due to quenched inhomogeneities, finite driving velocities, or dissipation.

A phenomenon which, to our knowledge, has not so far been addressed by dynamical models of the type cited above, is post-seismic relaxation [8]. It is commonly believed that viscoelastic relaxation in the immediate post-seismic period results in a redistribution of the loads, with delay times of the order of minutes, hours, or days [9]. The modelling of these processes should help us understand such empirical findings as, for example, "Omori's Law," which says that the frequency of occurrence of "aftershocks" decreases with time elapsed after the "main shock" as

$$n(t) \sim \frac{1}{(\text{const.} + t)^p} \quad , \qquad (1)$$

where p is usually found to be very close to unity [3,10].

In this paper, we mimick viscoelastic relaxation by introducing a finite stress transfer velocity into a dynamical model recently studied by Dahmen et al. [13], and we investigate its effects on the spatio-temporal behaviour of this simple model. In our coarse grained representation, we do not claim to model the precise microscopic mechanism for viscoelasticity, i.e., whether the relatively slow stress transfer actually comes from multiple brittle processes in a heterogenous medium [11] or from coupling to a viscous layer below the litosphere [12]. We will simply take the stress transfer velocity (V) to be some effective group velocity which governs post-event relaxation in the system and which is smaller than the velocity of sound [14].

The model we have used as our point of departure is an infinitely long range (Mean Field) version of the Ben-Zion and Rice [4] model which has been investigated both analytically and numerically [13], to reveal the presence of two different regimes as far as spatial and temporal distributions are concerned. It has been found, for a narrow distribution of heterogeneities, in the limit of infinitely slow drive, that the phase space can be described in terms of just two parameters, the dynamical weakening ϵ and conservation c, both taking values between 0 and 1. For $c < 1/2$ and small ϵ, the behaviour is critical; this is the so called Gutenberg-Richter (GR) regime, with a power law distribution of event sizes. For $c > 1/2$ and ϵ close to unity, one finds a metastable state of two-phase coexistance, with GR behaviour interrupted by stretches of quasi-periodic, characteristic (system-size) events, i.e. "runaway" behaviour.

Clearly, for the purely Abelian models that have so far been considered [7,13], just the retardation effect coming from the introduction of a finite velocity of stress transfer cannot make any difference in the overall statistics, since it does not matter in which sequence the sites are updated [15]. Therefore, the introduction of spatiality beyond that embodied in the mean field (infinitely long range) approximation had to be considered simultaneously with the retardation effect. Namely, the interactions strengths ("spring constants") were made to depend inversely on the distance, in keeping with a one-dimensional picture of the fault zone.

In this study we therefore consider simultaneously *i)*the effect of time delay in the transfer of stress, *ii)* the decay of the coupling strength with inverse distance, for the model of Dahmen et al. [13] in one dimension. We have moreover considered a slightly different distribution of heterogeneities.

We find that this new model leads to three distinct phases. The phase diagram is shown schematically in Fig. 1. The phase space has been probed over a grid of $\Delta c = 0.1$, for $\epsilon = 0, 0.5$ and 1. For strongly dissipative (c

near 0) systems with relatively weak "dynamical soften-ing" effects (ϵ close to 0) we find a GR-like phase, with very small events which show a very steep incipient power law behaviour over a rather narrow range of sizes and then cut off abruptly, and which display essentially no temporal correlations. The power spectrum of the event sequence is white-noise. For intermediate values of these parameters, the event distribution is similar to the first, however the power spectrum reveals non-trivial temporal correlations, a feature not observed by Dahmen et al. [13] in the GR phase. In the region of c close to unity (strong conservation) we find quasiperiodic runaway behaviour.
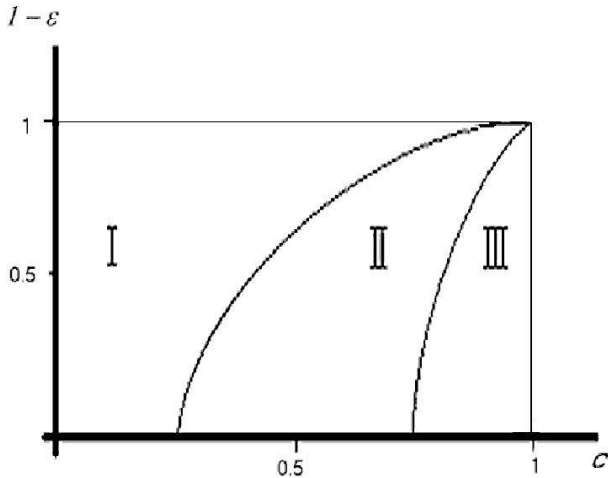

FIG. 1. Schematic phase diagram exhibiting three differ-ent "phases" where, I.) small events delta correlated in time, II.) small events with Cauchy type time correlations, and III.) quasiperiodic, system-size runaway events, dominate.

The phenomenology of each of these phases is rather rich. In regions of strong heterogeneity, one may ob-serve patches of blocks to slip in unison, pinned at ei-ther end by relatively large threshold stresses, exhibiting quasiperiodic behaviour within a sea of power law events. We have not observed the switching behaviour between coexisting GR and runaway phases, as reported for the mean field model [13], but this may be because this would require prohibitively long simulations in our scheme. The distribution of the accumulated stresses along the fault zone is both qualitatively and quantitatively similar in all the three regions, in contrast to the previous findings.

It should be stressed here that our approach is a de-parture from the usual quest for scale invariant spatial or temporal distributions. With the introduction of a fi-nite stress transfer velocity (which we take to be unity), and a finite driving velocity, we in fact have three well seperated time scales in the problem: That of the driv-ing velocity (the largest time scale), the viscoelastic time scale, and the triggering time scale (where slip occurs instantaneously).

The paper is organized as follows. In section 2, the precise definiton of the model is given. In section 3, we report our results for the statistics of the magnitudes in-tegrated over time scales corresponding to typical event durations, which should be compared with those in the infinite stress transfer velocity/zero driving velocity limit. We then go on to compute temporal and spatial correla-tion functions for coarse grained events. In section 4 we provide a discussion of our findings.

II. THE MODEL

We consider a one-dimensional array of finite segments, or blocks. The local stress τ_i on the ith block is given, at time t by

$$\tau_i(t) = \sum_{r=-R}^{R} k_r[u_{i+r}(t - r/V) - u_i(t)] + K[vt - u_i(t)]$$

(2)

where the range of the interaction, R, is of the order of the system size, $u_i(t)$ is the offset of the ith block in the direction of the constant driving velocity v, at time t; K is the effective shear modulus, and $k_r = k/|r|$ is the elastic coupling between blocks seperated by a distance r. As long as all the $\tau_i < \tau_{s,i}$, where $\{\tau_{s,i}\}$ are randomly distributed failure stresses, the system is immobile.

The viscoelastic stress relaxation is mimicked by the delay, r/V, in the transfer of stress. We shall henceforth set V, the velocity for the stress transfer along the blocks, to unity. Note that V is not typically the sound veloc-ity, but some effective group velocity smaller than that of sound, governing the processes of viscoelastic stress relaxation in this coarse grained model. [8,14]

The dynamics is defined as follows. If the threshold value is exceeded at some i, at time t, then

i) The stress at the ith block is reduced by

$$\delta\tau_i = \tau_{s,i} - \tau_{a,i} \ , \tag{3}$$

where the $\{\tau_{a,i}\}$ are random arrest stresses.

ii) The value of the failure stress at the i'th block is re-set, until all motion once more ceases, to a "dynamical" threshold value

$$\tau_{d,i} = \tau_{s,i} - \epsilon(\tau_{s,i} - \tau_{a,i}) \ , \tag{4}$$

where ϵ parameterizes the dynamical weakening effect.

iii) The stress drop is redistributed, according to Eq.(2), so that τ_{i+r} is incremented, at the $t + |r|$'th time step by

$$\delta\tau_{i+r} = c_r(\tau_{s,i} - \tau_{a,i}) \qquad c_r = \frac{k_r}{\sum_{r'} k_{r'} + K} \tag{5}$$

We may once more define $c \equiv \sum_r c_r$, with $0 \le c \le 1$, to be the parameter which measures the degree of conserva-tiveness of the system, although it should be noted that

2

this definition now involves an implicit integral over time as well as space.

The boundary conditions are fixed, so that $u_1 = u_L \equiv 0$. At each time step, the stress at all the blocks i is recalculated according to Eq.(2). This means that the constant drive term Kvt is incremented also.

III. SIMULATIONS

Since the finite stress transfer velocity introduces a definite time scale into the system, which also sets the characteristic time scale of the event duration, one now faces the problem of having to go to extremely long runs with a driving velocity which is at least six to seven orders
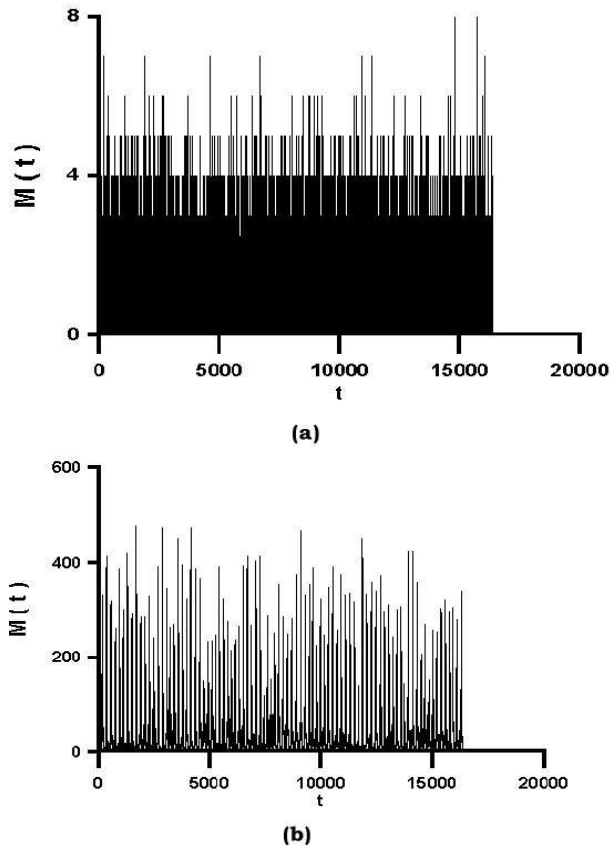

(a)

(b)

FIG. 2. Typical time series for the magnitudes M v.s. time, for 16384×128 time steps. a) in the "Gutenberg-Richter" (small event) and b) the runaway regimes. Note the difference in the vertical scales. Shown are plots for a) $c = 0.16$, $\epsilon = 0.5$; b) $c = 0.9$, $\epsilon = 0.5$. The driving velocity is $v = 10^{-5}$ and the shear modulus $K = 1$ for this and the following figures.

of magnitude smaller than the latter. The zero driving velocity trick of simply scanning the system for that site which is closest to slipping and loading all sites by the missing amount, is no longer appropriate here - one has to first check that there are no stress "parcels" still on

the way. The actual simulation times get prohibitively large as a result, and we had to be content with large but finite ranges of interaction, up to 1/6 the fault size, and with a one-dimensional fault.

Table I.

Values of the Gutenberg-Richter exponent b in the different regimes.

Region	c	ϵ	b
I	0.15	0.5	5.2
II	0.65	0.5	5.2
III	0.9	0.5	1.6

We have simulated the system described in the preceding section on a grid of 300 blocks, with the range of interactions going up to $R = 50$. The distribution of stress drops $\delta\tau_i = \tau_{s,i} - \tau_{a,i}$ was chosen to have the form $p(x) \propto x^{-\mu}$, with $\mu = 1.2$ However, upon finding that arbitrarily large stress drops pinned the edges of finite segments in the fault and distorted the distribution of event sizes, we decided to limit the range of the $\delta\tau$ to a width comparable to those considered in Ref. ([13]), namely 0.2. It is generally found that long active fault zones organize themselves into states with relatively small heterogeneity, and our results should be considered in this spirit.

The driving velocity v is taken to be $10^{-5}V$ in the simulations reported below. It should be noted that larger driving velocities result in individual cells exceeding their threshold values and collapsing independently from their neighbors, and as a result the system never achieving a self organized state. With realistic driving velocities of $\sim 10^{-9}$ m/sec, $v = 10^{-5}V$ corresponds to a stress transfer velocity of $\sim 10^{-4}$ m/sec. For "block sizes" of $\sim 10^2$ meters setting our lattice spacing, a stress transfer velocity of $V \sim 10^{-4}$m/s corresponds to time steps of duration 10^6 s.

In Figure 2, we display the typical time series resulting from plotting the integrated magnitudes $M(t)$ for different values of the system parameters. These are obtained by summing over the number of blocks where the threshold has been exceeded within an interval $\delta t = 128$.
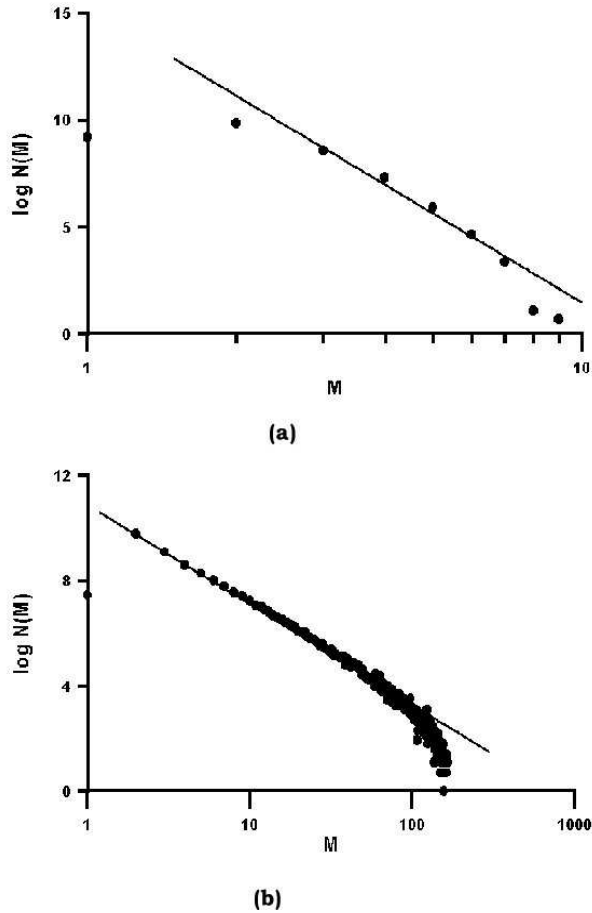
3

(a)

(b)

FIG. 3. The frequency v.s. magnitude plots on a double logarithmic scale, for the same set of parameters as a) and b) in Figure 2. The lines are intended as a guide to the eye with slopes -5.2 and -1.6, respectively.

This value was chosen as approximately that time interval needed for a signal originating in the middle of the fault to be able to reach the edges of the fault. This time-coarse- grained way of identifying events is in keeping with the way earthquake data is taken, with the time integral taken over the actual displacements of the seismographs. Thus, we define,

$$M(t) = \sum_{t'=t}^{t+\delta t} \sum_{i} [\Delta u_i(t')]^0 \quad , \tag{6}$$

where the zeroth power of the slip $\Delta u_i(t')$ is taken so that $M(t)$ simply counts the number of slipped blocks within the time interval δt. The time series $M(t)$ reveal no immediately observable differences between the regions I and II shown in Fig.1; therefore we have selected only one set of parameter values to illustrate both these regions (see Fig. 2a). On the other hand the much larger magnitudes observed in the runaway region, and their marked quasiperiodicity are apparent in Fig. 2b.

The regions I and II are also similar in the way the frequency $f(M)$ of events scales with the magnitude M, for a given binning size δt. In Figure 3, we show the plots of the frequency $f(M)$ v.s. magnitude M in the small event (the "Gutenberg-Richter" phase found in Ref. [13]) and in the runaway regime, for the same parameter values as in Fig. 2. The "power law" fits, $f(M) \sim M^{-b}$, to the small event regime (regions I and II) are poor, and can only be thought of as suggestive; they extend over too small a range to really signify self–similarity. Notice that in the "runaway" regime (region III), the magnitudes cover a wider range; however we do not observe as marked a "super-criticality," i.e., a frequency of *large* events in excess of a power law size distribution, as has been reported elsewhere [3,4,18].
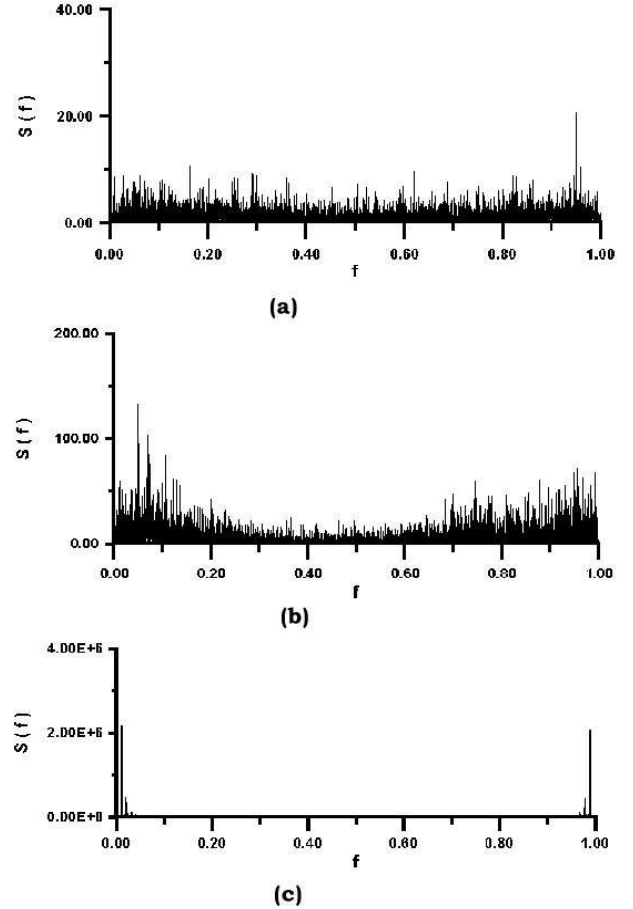

(a)

(b)

(c)

FIG. 4. Power spectra of the time series of magnitudes, computed for parameter values in the regions I, II, III of the phase diagram shown in Fig.(1). a) $c = 0.16$, $\epsilon = 0.5$, b) $c = 0.72$, $\epsilon = 0.5$, c) $c = 0.89$, $\epsilon = 0.5$. The data for panels a) and c) are taken over series of 8192×128 time steps. The data in panel (b) have been averaged over 7 runs of 16384×128 time steps.

Within regions I and II, the Gutenberg-Richter exponent b is sensitive to the driving velocity v and also depends, less strongly, on the parameters c, ϵ. Here the distribution is very steep, with b ranging between 4 and 5. The values obtained are given in Table I. The "runaway"

regime exhibits much more realistic b values, around 1.5 to 1.6. One should note, moreover, that since the system is no longer scale invariant, the statistics of the magnitudes M are also sensitive to the binning size δt, so that the b values here are only useful for purposes of discriminating between different regions of the phase space.

The interesting difference between the three regimes delienated in Fig. 1 become apparent in the power spectra,

$$S(f) = \int dt e^{i2\pi ft} C(t) \quad , \tag{7}$$

where

$$C(t) = \frac{1}{T} \int_0^T dt' M(t') M(t' + t) \tag{8}$$

is the time-correlation function for the coarse grained magnitudes $M(t)$, where t stands for the number of time intervals δt, for a total time of measurement extending over a period T.
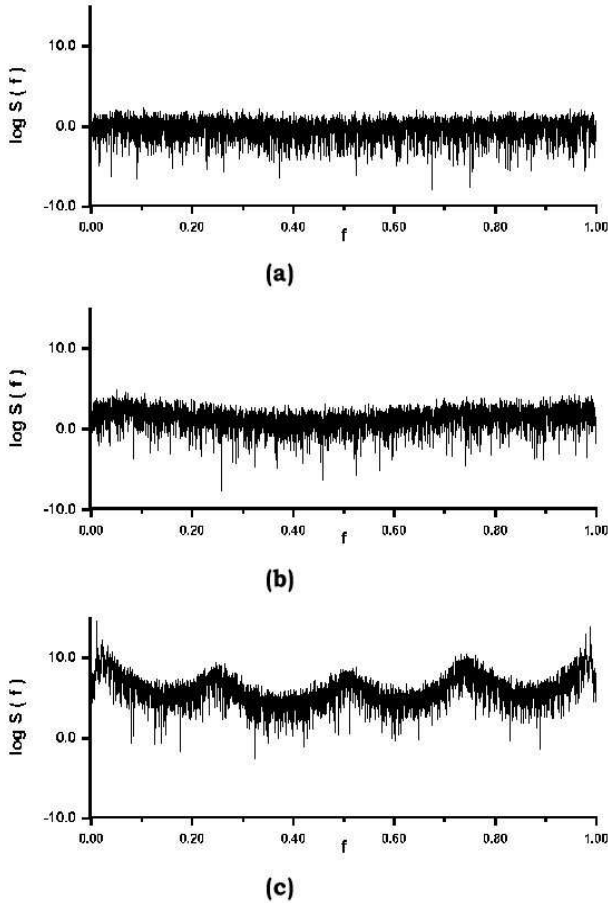

(a)

(b)

(c)

FIG. 5. The same power spectra as in Fig. 4, on a logarithmic scale. Panels a), b), and c) belong to the regions I, II, III of the phase diagram in Fig. 1.

In Figures 4 and 5 we display linear and semi-logarithmic plots of the power spectrum in the three different phases. It can be seen in Fig.(4a) and in a more pronounced way in the logarithmic plot of the same power spectrum in Fig.(5a) that in the "small event" regime I (panel a), the power spectrum is essentially flat, white-noise like, indicating an absence of correlations between the earthquakes, i.e., $C(t) \propto \delta(t)$. For intermediate values of c and ϵ, i.e., in the small-event region II, however, we find that superposed upon the white-noise like background, the upper envelope of the power spectrum displays a distinctive curve, (see Fig.4b) indicating the presence of non-trivial temporal correlations. In the runaway region (region III), we find a markedly different, quasiperiodic behaviour, as can be see from Figs. (4c) and (5c). The very pronounced peak in the power spectrum near the origin is large enough to suppress all the others; we can see the other frequencies that are present only in the logarithmic plot.

In Figure 6, we show the result of taking an inverse transform of the *envelope* (roughly the highest points) of the power spectrum shown in Fig. 4b. This crude estimate of the time correlation function is corraborated by a more careful evaluation, to which we now turn.
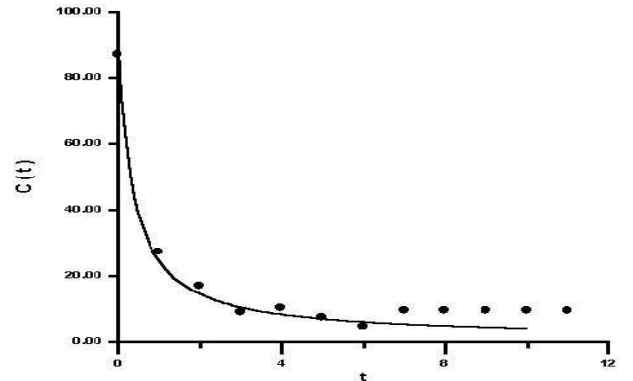

FIG. 6. A crude estimate for the time correlation function, from the inverse Fourier transform of the points in the envelope of the power spectrum, shown in Fig. 4b. The fit is to $1 + 85(1 + 3t)^{-1}$.

We have computed $C(t)$ directly from a time series of 81920 time intervals (of 128 steps each). We have normalized the correlation function by $(1/T) \int_0^T M^2(t')dt'$, so that $C(0) = 1$. We find that the normalised $C(t)$ can be fit rather well by a function of the form
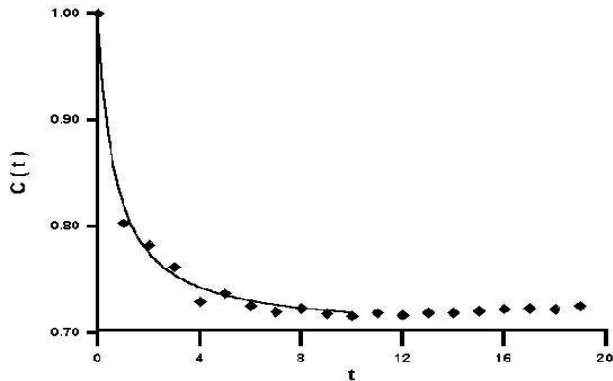
$$C(t) = A + \frac{B}{D + t} \quad , \tag{9}$$

FIG. 7. The time correlation function $C(t)$ in region II of the phase diagram ($c = 0.65$, $\epsilon = 0.5$), computed from Eq.(8), over a time series of 81920×128 steps. The fit is to $0.7 + 0.2(0.66 + t)^{-1}$.

with $A = 0.7$, $B = 1/5$, $D = 2/3$. Our results are shown in Fig.7.

Note that the time correlation function $C(t)$ measures the average frequency with which a time lapse t seperates two events, *weighted* by the magnitude of the events. In another way of saying the same thing, it is the weighted average of the number of times that one registers pairs of events seperated by a time lapse equal to t. If there is no event taking place at time $t + t'$ after an event at time t', i.e., if $M(t') \neq 0$, but $M(t + t') = 0$, there will be no contribution to the integral for $C(t)$ in (8).

We would like to recall, at this point, Omori's Law (1) for the frequency of aftershocks [3,10]. Actually, geophysicists are generally hesitant to label a given shock as either an "aftershock" or "main schock," and admit that these are conventional distinctions, which are difficult to make precise in a quantitative way. Viewed in this way, Omori's law is just a statement of the relative frequency of pairs of events seperated by a time t, and is a slightly cruder version of the time correlation function. We see that the form we find for the time-decay of the correlation function matches that of Omori's Law, with a power $p = 1$, as found for real earthquake statistics.

From Fig. 7, and Eq.(9), we see that $C(t) - A$ drops by a factor of $1/2$ within one time interval (consisting of 128 time steps). Since we have already estimated the time steps here to correspond to about 10^6 seconds, this means correlations times of the order of 10^8 s, namely ~ 3 yrs, which is quite realistic for the time interval in which aftershocks die away after a big event.
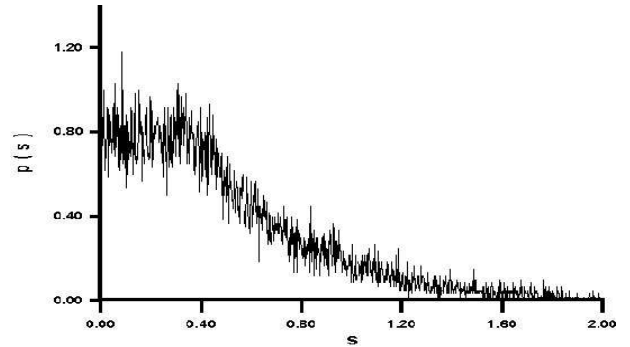

FIG. 8. The probability density of the fraction s of the slipping stress (see text) computed along the fault zone, for $c = 0.89$, $\epsilon = 0.5$ (region III). The histogram is averaged over 20 snapshots, seperated by 5×10^4 timesteps. The figures for regions I and II are indistinguishable from this one.

To investigate the spatial correlations in the system, we first considered the distribution of the fraction of the slipping stress on each block,

$$s_i \equiv \frac{\tau_{s,i} - \tau_i}{\langle \tau_{s,i} - \tau_{a,i} \rangle} \quad , \qquad (10)$$

along the fault zone. This is a quantity in which one might have expected a greater self-organization building up as one goes from region I to region III in the phase diagram, yet we did not find this to be the case. In contrast to Ref. [13], in the present model the distribution $p(s)$ remains essentially invariant in all the three regions, and has the shape shown in Fig. 8. Similarly, we found that the equal time spatial correlations $\langle s_i s_{i+r} \rangle$ between the fraction of the slipping stresses accumulated at each site, showed essentially delta function behaviour in all three regions, with the correlations never extending beyond next nearest neighbors. On the other hand, defining the coarse grained toppling variables

$$m_c(t, i) \equiv \sum_{t'=t}^{t+\delta t} [\Delta u_i(t')]^0 \quad , \qquad (11)$$

and setting $m_c(i) = 0$ at sites beyond the boundaries of the fault we found that the correlation function

$$C_m(r) = \frac{\langle m_c(t,i) m_c(t,i+r) \rangle - \langle m_c(t,i) \rangle^2}{\langle m_c(t,i) \rangle^2} \quad , \qquad (12)$$

where the averages are performed both over i and t, indeed displayed markedly different behaviour in region III, in comparison to I and II. Our results are shown in Fig. 9. The time averages were performed over 60 snapshots, taken at intervals of 5×10^4 timesteps. The correlations are negligible (of the order of 10^{-4}) in the first two regions, whereas, in region III, one sees a gradual decay. A straight line fit to the semilogarithmic plot (Fig. 10) suggests an exponential decay and gives a correlation length of 30 lattice units, corresponding to $\sim 3 \times 10^3$ meters.
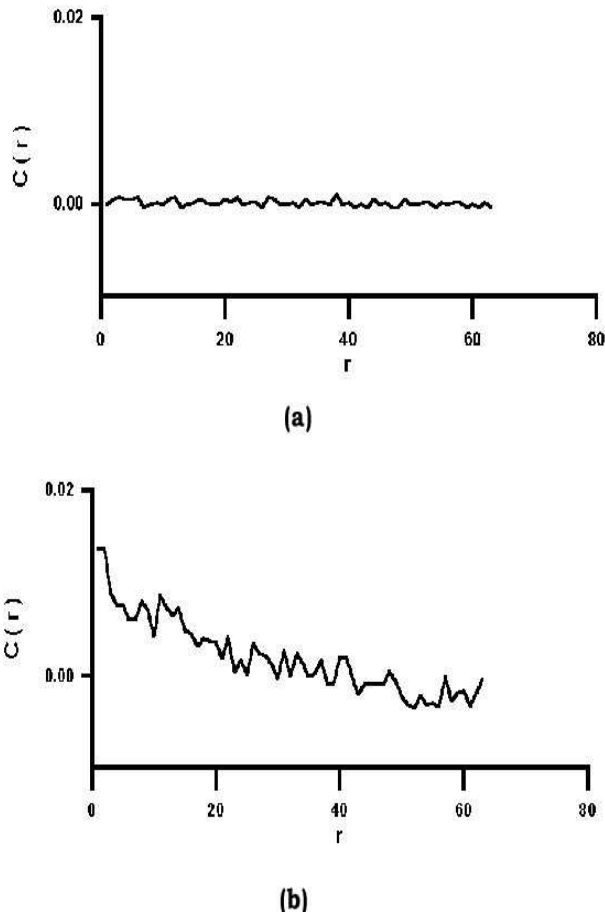
6

(a)

(b)

FIG. 9. The spatial correlations between toppling events coarse grained in time, in the regions I and III of the phase diagram. a) $c = 0.16$, $\epsilon = 0.5$, b) $c = 0.89$, $\epsilon = 0.5$. The plot for $c = 0.54$, $\epsilon = 0.5$ (in region II) looks identical to panel a). Averages have been taken over 60 snapshots seperated by time intervals of 50,000 steps.

IV. DISCUSSION

The inclusion of viscoleastic effects into the study of crack propagation and pinned driven systems has recently made important progress [16,17], and promises to be fruitful also in the modeling of earthquakes. The most important outcome of introducing viscoelastic effects is to be found in the more subtle temporal correlations between events; for highly dissipative systems the correlations are delta function like, whereas for intermediate values of the dissipation, one observes correlations that decay as $\sim (\text{const.} + t)^{-1}$ between events, which is of the form of Omori's Law (1). To our knowledge, this is the first demonstration of how Omori's Law may arise in such a system.

Our preliminary findings indicate that, due to viscoelastic effects, the runaway phase (region III) of quasiperiodic events in the present model of a heterogeneous fault zone is pushed to a relatively smaller region of the phase diagram (see Fig. 1) than found previously [13] and the frequency distribution in this phase displays scale invariance over a sizable region of event sizes. We have verified that this region is distinguished by relatively long range spatial correlations between slipping events, in contrast to the "small event" regimes.
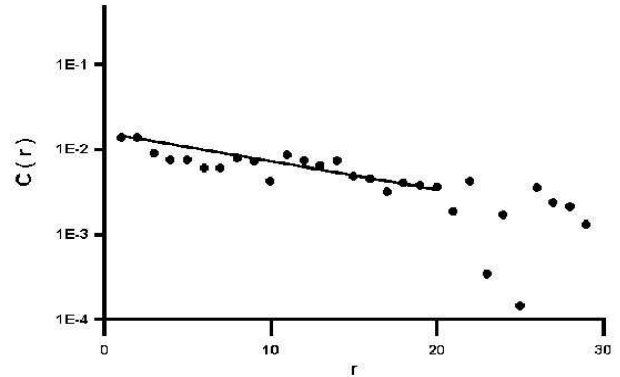

FIG. 10. Semilogarithmic plot of the spatial correlations in region III. The slope of the straight line fit gives a correlation length of 30 lattice units, or equivalently, 3×10^3 meters.

It has been remarked before [3,18] that various system-dependent features, notably dynamical weakening and dissipation, introduce time and length scales into the problem and take the system away from criticality. We would like to remark that one may reverse the emphasis here to say that rather than the scaling region of the Gutenberg-Richter regime, one should examine the sub– or super–critical behaviour to characterise a specific fault zone. In particular, we have shown that determining the nature of the space and time-correlations in the system gives important clues as to the relative degree of dissipation or dynamical weakening.

[1] R. Burridge and L. Knopoff, Bull. Seismo. Soc. Am., **57**, 341 (1976).
[2] J.M. Carlson, J.S. Langer, B.E. Shaw, Rev. Mod. Phys. **66**, 657 (1994).
[3] I. Main, Reviews of Geophysics, **34**, 433 (1996).
[4] Y. Ben-Zion and J.R. Rice, J. Geophys. Res. **98**, 14109 (1993); J. Geophys. Res. **100**, 12 959(1995); J. Geophys. Res. **101**, 5677 (1996).
[5] P. Bak and C. Tang, J. Geophys. Res. **94**, 15635 (1989).

[6] D. Sornette and A. Sornette, Europhys. Lett. **9**, 197 (1989).

[7] Z. Olami, H.J.S. Feder, and K. Christensen, Phys. Rev. Lett., **68**, 1244 (1992).

[8] C.H. Scholz, *The Mechanics of Earhquakes and Faulting* (Cambridge University Press, Cambridge, 1990).

[9] Ibid., p. 314ff.

[10] Ibid., p. 205.

[11] Ibid., p. 34.

[12] Ibid., p. 236.

[13] K. Dahmen, D. Ertaş, and Y. Ben-Zion, Phys. Re. E **58**, 1494 (1998).

[14] Y.T. Chen and L. Knopoff, "The quasistatic extension of shear crack in a viscoelastic medium," Geophys. J. R. astr. Soc. **87**, 1025 (1986).

[15] D. Dhar, Phys. Rev. Lett. **64**, 1613 (1990).

[16] D.A. Kessler and Levine, Phys. Re. E **59**, 5154 (1998).

[17] M.C. Marchetti, A.A. Middleton, T. Prellberg, "Viscoelastic depinning of driven systems: mean field plastic scallops," cond-mat/9912461.

[18] M. Anghel, W. Klein, J.B. Rundle, J. S. Sá Martins, "Scaling in a Cellular Automaton Model of Earthquake Faults," cond-mat/0002459.